

LA-7140

c.3

UC-45

Issued: May 1978

**REPRODUCTION  
COPY**

**IS-4 REPORT SECTION**

**Characterization of Two Commercial Explosives**

B. G. Craig  
J. N. Johnson  
C. L. Mader  
G. F. Lederman

LOS ALAMOS NATIONAL LABORATORY  
3 9338 00311 9152

**los alamos**  
**scientific laboratory**

of the University of California

LOS ALAMOS, NEW MEXICO 87545

An Affirmative Action/Equal Opportunity Employer

UNITED STATES  
DEPARTMENT OF ENERGY  
CONTRACT W-7405-ENG. 36

This work was supported by the US Department of Energy,  
 Division of Oil, Gas, Shale, and In Situ Technology.

Printed in the United States of America. Available from  
 National Technical Information Service  
 U.S. Department of Commerce  
 5285 Port Royal Road  
 Springfield, VA 22161

Microfiche \$ 3.00

001-025	4.00	126-150	7.25	251-275	10.75	376-400	13.00	501-525	15.25
026-050	4.50	151-175	8.00	276-300	11.00	401-425	13.25	526-550	15.50
051-075	5.25	176-200	9.00	301-325	11.75	426-450	14.00	551-575	16.25
076-100	6.00	201-225	9.25	326-350	12.00	451-475	14.50	576-600	16.50
101-125	6.50	226-250	9.50	351-375	12.50	476-500	15.00	601-up	-- 1

1. Add \$2.50 for each additional 100-page increment from 601 pages up.

This report was prepared as an account of work sponsored by the United States Government. Neither the United States nor the United States Department of Energy, nor any of their employees, nor any of their contractors, subcontractors, or their employees, makes any warranty, express or implied, or assumes any legal liability or responsibility for the accuracy, completeness, or usefulness of any information, apparatus, product, or process disclosed, or represents that its use would not infringe privately owned rights.

CONTENTS

ABSTRACT..... 1

I. INTRODUCTION..... 1

II. PRELIMINARY EXPERIMENTS..... 2

III. WATER-TANK EXPERIMENTS..... 3

    A. Experimental Techniques..... 4

    B. General Analysis of the Experiment..... 5

    C. Experimental Results for ANFO and WGE-1..... 7

IV. NONIDEAL EXPLOSIVES AND THEORETICAL SIMULATION  
OF THE WATER-TANK EXPERIMENTS..... 11

    A. ANFO..... 12

    B. WGE-1..... 14

V. CONCLUSIONS..... 15

ACKNOWLEDGMENTS..... 16

APPENDIX. INDEX-OF-REFRACTION EFFECTS..... 16

REFERENCES..... 18



## CHARACTERIZATION OF TWO COMMERCIAL EXPLOSIVES

by

B. G. Craig, J. N. Johnson, C. L. Mader  
and G. F. Lederman

### ABSTRACT

Experimental data are obtained for the performance of two commercial explosives, an ammonium-nitrate/fuel-oil mixture (ANFO) and a water-gel explosive (WGE-1), using the water-tank, or aquarium, technique. Plexiglas and clay tubes (10- and 20-cm-diam) containing the explosive are submerged in a large transparent water tank. The explosive system is detonated from the top and an image intensifier camera records the shock wave in water as well as the dynamic expansion of the confining cylinder. The experimental data are compared with two-dimensional Lagrangian hydrodynamic calculations based on various assumptions regarding nonideal explosive behavior. The results show that substantial fractions (30 to 50%) of the constituents do not participate in the chemical reaction at the detonation front. For ANFO, complete reaction takes place within a few microseconds behind the detonation front. For WGE-1, detectable additional reaction does not occur within experimental recording time ( $>200 \mu\text{s}$ ). These results have important applications in effective rock breakage with commercial explosives.

### I. INTRODUCTION

A subject of current national interest is energy and mineral resource recovery, and an important part of this subject is controlled rock blasting with commercial explosives. Explosive rock blasting has been studied empirically by a number of investigators.<sup>1-5</sup> Generally, these studies consist of developing a data base for empirical relationships between rock blasting efficiency and detonation velocity, energy release, expansion work, etc. The reason for such an approach is that detailed consideration of actual explosive performance, coupled with high-, intermediate-, and low-strain-rate fracture mechanics to predict actual removal of rock from a blasting face, is an extremely difficult problem. However, as our predictive capabilities in dynamic rock fracture improve, we need more detailed information about the behavior of the explosives involved.

Many explosives systems have been studied extensively and their behavior is extremely well understood. However, when explosive performance

closely follows theoretical behavior (we say the explosive behaves ideally), economic considerations often limit its applicability because of the cost of the great quantities of explosive needed on a commercial scale. But commercially available explosives often do not behave according to steady-state theoretical predictions based on equilibrium thermodynamics of the expected detonation products (such explosives have nonideal behavior). Therefore, for nonideal commercial explosive systems, extensive measurement of several performance parameters are necessary to assess correctly the actual behavior and departure from ideal conditions.

In this report we present experimental and theoretical results for the characterization of two commercial explosives: ANFO (ammonium nitrate/fuel oil, approximately 94 wt%/6 wt%) and a water-gel explosive (approximately 46 wt% ammonium nitrate, 24 wt% TNT, 15 wt% sodium nitrate, 13.2 wt% water, 1.2 wt% ethylene glycol, and 0.6 wt% thickener) that we shall call WGE-1. The densities of ANFO and WGE-1 are nominally  $0.9 \text{ g/cm}^3$  and  $1.5 \text{ g/cm}^3$ , respectively.

Results of preliminary rate-stick experiments are initially presented to bracket the performance of both explosive systems; that is, to determine how confinement and charge diameter influence production of high-order detonation and how various booster systems affect performance. This is then followed by a comprehensive discussion of data obtained in aquarium, or water-tank, experiments in which 10- and 20-cm cylindrical charges of ANFO and WGE-1 (all  $\sim 100$  cm long) are observed optically following detonation from one end. The data consist of measured radial positions of the confinement tube and the water shock as functions of position behind the detonation front. Two-dimensional hydrodynamic calculations of the aquarium shots are then performed and compared with experimental data, giving considerable information on the actual performance of these two explosive systems. This method is similar to that used in performance studies of other nonideal explosive systems.<sup>6-11</sup>

The final results are estimates of the degree of ammonium-nitrate (AN) reaction at and immediately behind the detonation front as a function of charge diameter. We expect this study to improve our understanding of nonideal explosives, in general, and of two commercial explosives, in detail. Our goal is better descriptions of explosive rock breakage based on first principles.

## II. PRELIMINARY EXPERIMENTS

ANFO was chosen as the first explosive to study because of its low cost, desirable safety, and widespread use. However, as mentioned in Sec. I, ANFO is a nonideal explosive; that is, its performance depends on the charge diameter, length, and confinement. Some of these variables have been investigated by several researchers,<sup>7,8,12,13</sup> and so we will compare our newly generated data and the existing data. In addition, its performance near the booster (perhaps for several meters from the booster) depends on how it is boosted. These variables lead to major complications in modeling the performance and result in unusual experimental requirements.

We need a model that will describe the performance in a typical borehole and that allows for variations that result from the material in which the hole is located, the hole diameter and length, how

the charge is boosted, how the charge is stemmed, and the distance to a free face or other boreholes. The quantitative effect of each of these variables and their combinations on the performance of ANFO needs to be understood.

The total cost of rock fragmentation will be significantly influenced by the cost of boreholes, which increases with the hole diameter. Better control of rubble size can be expected for smaller and more numerous holes, all other parameters being equal. Generally, the smallest borehole used with ANFO is about 7.6 cm (3 in.) in diameter; however, economics or practical requirements may force the use of a borehole as large as 10.2 cm (4 in.) in diameter. One practical requirement for modeling is that the ANFO detonate high order. A low-order, or low-velocity, detonation may break rock but does not lend itself to modeling; a nonideal high-order detonation will be difficult enough. We must calibrate our model to a range of borehole diameters that meet the above requirements.

The most economical way to load ANFO into numerous boreholes is with a pneumatic loader. Pneumatic loading gives a density of  $\sim 0.98$  g/cm<sup>3</sup> as opposed to  $\sim 0.80$  g/cm<sup>3</sup> for pour loading. Our model should be calibrated to a density representative of that obtained with pneumatic loading. Incremental loading of ANFO into a tube while it is appropriately vibrated gave the desired densities.

Ionization and mechanical switches for measuring the progress of the reaction were first tested with granulated TNT and then with ANFO. Ionization switches, two lengths of 1.59-mm-diam stainless steel welding rod separated by 1 mm, are able to withstand the loading operation without deflection and respond to a high-order but not a low-order detonation. A coaxial mechanical switch of existing design responded to either high- or low-order detonation and to shock waves in water when the shock pressure is as low as 0.1 to 0.2 GPa (0.1 GPa = 1 kbar).

Table I summarizes the results of our analytical and hazard testing on ANFO.

The results of standard rate-stick experiments with ANFO show that it does not propagate a high-order detonation in a 7.6-cm-diam stick confined

TABLE I  
NOMINAL PROPERTIES OF ANFO<sup>a</sup>

<u>Composition</u>	<u>Wt Per Cent</u>
No. 2 diesel fuel oil	6.27
NH <sub>4</sub> NO <sub>3</sub>	93.73 (by difference)
<u>Impact Sensitivity Test</u>	<u>Result</u>
Type 12	1 explosion out of 10 at 320 cm
Type 12B	None at 320 cm
<u>Stability</u>	<u>Result</u>
Vacuum	<0.1 ml/g at 120°C in 48 h
DTA <sup>b</sup>	Normal for NH <sub>4</sub> NO <sub>3</sub>
Pyrolysis	Normal for NH <sub>4</sub> NO <sub>3</sub>

<sup>a</sup>Nitro-Carbo-Nitrate Blasting Agent, Gulf Oil Chemical Company, lot GOC 657A051976, specification Spe N-C-N1, pink, \$0.12/lb.

<sup>b</sup>Differential thermal analysis.

with 0.63-cm-thick Plexiglas\* or 0.5-cm-thick Pyrex,\*\* even when the charge is strongly overboosted with a plane-wave lens plus 2.5-cm-thick Composition B (CB). The overdriven detonation slowed to low order within 1 diam of run. Confining materials such as Dural were rejected because their sound speeds exceed the detonation velocity of ANFO and thus influence explosive performance.

A shot (E-4266) was prepared with ANFO loaded into a Plexiglas tube of 10.1-cm i.d. and 0.63-cm wall thickness. The booster was a P-40 Baratol plane-wave lens plus a 2.5-cm-thick CB slab in contact with the ANFO mixture. Ionization switches were located every 5 cm along the tube (61-cm-long) beginning 10 cm from the booster/ANFO interface. The ANFO density ( $\rho$ ) was 0.964 g/cm<sup>3</sup> and the temperature at firing time was 27°C. Detonation was high order. The detonation velocity (D) at the charge axis was 4.9 km/s over the first 10 cm and slowed to a steady-state value of 3.39 ± 0.02 km/s after a run of 3.5 charge diam. The detonation velocity along a line 1.2 cm inside the edge of the charge was also initially overdriven and slowed to the same steady-state value after a run of 3.5

\*Rohm and Haas GMBH, Darmstadt, Germany.  
\*\*Corning Glass Works, Corning, NY 14830.

charge diam. The steady-state velocity observed is less than that reported for ANFO prills confined in a 5.2-cm steel tube (~3.7 km/s for the same density) but higher than reported for crushed prills in a 2.15-cm-diam steel tube (~3.2 km/s).<sup>14</sup>

A shot (E-4275) was prepared with ANFO ( $\rho = 0.950$  g/cm<sup>3</sup>), loaded into a nominal 8.8-cm-i.d., 0.63-cm-thick-wall tube of Plexiglas and with a booster identical to that in shot E-4266. When fired at 24°C, the overdriven detonation slowed from 4.52 km/s over the first 10 cm to a steady-state 3.02 km/s after 6 charge diam of run.

The results of all rate-stick experiments on ANFO are summarized in Table II. Shots F-3971, E-3975, E-3977, E-4272, E-4275, E-4274, and E-4266, in conjunction with minor auxiliary experiments, verified that a minimum diameter of 10 cm was required to sustain a high-order detonation ( $D \approx 3.4$  km/s) in a 0.6-cm Plexiglas confinement. Shots E-4266, E-4278, and E-4281 showed that booster overdrive becomes unimportant after a suitable length of run. Shot E-4300 showed that the effect of the confinement material, although minor, is real and must be considered.

Table III presents the results of similar experiments conducted on the WGE-1 system. Note that the sample diameter and type of confinement do not significantly alter the performance. The detonation velocity remains nearly constant at 4.83 to 4.86 km/s.

### III. WATER-TANK EXPERIMENTS

The rate-stick experiments described in Sec. II give detonation velocity as well as information on the effects of confinement and charge diameter, but they do not provide a quantitative understanding of the physical and chemical phenomena occurring behind the detonation front. Therefore, the water-tank experiment was developed to measure simultaneously detonation velocity and pressure, confinement effects, and the release isentrope from the Chapman-Jouguet (C-J) state.

In the following discussion we present (a) the detailed experimental techniques, (b) an analysis of measurement accuracy to be expected by this technique and the results of a proof test with PBX 9407,

TABLE II  
ANFO RATE-STICK EXPERIMENT SUMMARY

Shot No.	Booster System	i.d. [cm (in.)]	$\rho$ (g/cm <sup>3</sup> )	Length (cm)	D (km/s)	Comments
F-3971	Tetryl/TNT	7.6(3)	0.967	50	2.9 (?)	low-order, 0.6-cm Plexiglas confinement
E-3975	Tetryl/TNT	7.6(3)	0.964	50	3.0 (?)	low order, 0.5-cm Pyrex confinement
F-3977	P-40/CB	7.6(3)	0.972	50	2.8 at $\sim$ 25 cm and decaying rapidly	low order, 0.6-cm Plexiglas confinement
E-4272	P-40/CB	8.8(3.5)	0.953	75		no test
E-4275	P-40/CB	8.8(3.5)	0.950	75	4.5 at 10 cm 3.1 at 25 cm 3.0 at 50 cm 3.0 at 75 cm	signals decaying, borderline low-high order; 0.6-cm Plexiglas confinement
E-4274	P-40/TNT	10(4)	0.947	75		no test
E-4266	P-40/CB	10(4)	0.964	75	4.9 at 10 cm 4.6 at 25 cm 3.39 at 75 cm	high order, 0.6-cm Plexiglas confinement
E-4278	P-40/TNT	10(4)	0.960	75	3.5 at 25 cm 3.3 at 50 cm 3.3 at 75 cm	high order, 0.6-cm Plexiglas confinement
E-4281	Tetryl/TNT	10(4)	0.945	75	3.4 at 25 cm 3.3 at 50 cm 3.3 at 75 cm	some overboost at booster/ANFO interface, high order; 0.6-cm Plexiglas confinement
E-4288	P-40/TNT	$\sim$ 10( $\sim$ 4)	0.947	75		no test
E-4300	P-40/TNT	9.8(3.9)	0.909	75	3.6 (ion pins) 3.5 (mech. pins) after 2 diam	high order, 1.6-cm clay-pipe confinement
E-4307	Tetryl/TNT	9.8(3.9)	0.926	25		1.6-cm clay-pipe confinement

TABLE III  
WGE-1 RATE-STICK EXPERIMENT SUMMARY

Shot No.	Confinement	Booster System	Length (cm)	Diam (cm)	$\rho$ (g/cm <sup>3</sup> )	D (km/s)	Comments
E-4322	0.6-cm Plexiglas	P-40/CB	39.3	8.79	1.49	4.83	velocity given is average over entire length of rate stick
E-4327	0.32-cm Plexiglas	SE-1/Tetryl/CB	122.0	19.79	1.48	4.85	velocity given is for last meter of run
E-4336	2.22-cm clay	SE-1/Tetryl/CB	167.3	19.85	1.51	4.86	clay pipe has $\rho \approx 2.3$ g/cm <sup>3</sup>

and (c) experimental data for ANFO and WGE-1 of several diameters and confinements.

#### A. Experimental Techniques

The proceeding detonation wave, high-explosive (HE) water shock, and water on the confinement-tube/water interface were observed with a multiple-exposure, image-intensifier camera (I<sup>2</sup>C) manufactured

at Los Alamos Scientific Laboratory. The 40-mm image-intensifier tube can resolve  $\sim$ 16 line pairs/mm over the whole frame and has a useful light gain of  $\sim$ 625. The exposure times in the water-tank experiments on ANFO and WGE-1 are  $\sim$ 175 ns. Photo floods with four Fresnel lenses are used for back-lighting the image. A complete description of this

experimental apparatus is given by Winalow, Davis, and Chiles.<sup>15</sup>

### B. General Analysis of the Experiment

Figure 1 shows a schematic diagram of the experimental setup for the HE/water-tank experiments. A cylinder of explosive is detonated from the top in a transparent confining medium, and we measure the radial positions of the bubble and shock waves in the fluid as functions of distance behind the detonation front. The following question is then asked: What is the sensitivity of these measurements to differences in basic detonation parameters; that is, do these measurements give sufficiently accurate information on detonation properties in addition to the detonation velocity?

To answer this question, two-dimensional Lagrangian hydrodynamic calculations<sup>16,17</sup> are performed (using code 2DL) on a hypothetical 15-cm-diam cylindrical explosive in water with an initial density of  $1\text{ g/cm}^3$  and a detonation velocity of 4.6 km/s. We assume that the explosive products obey a gamma-law equation of state with a variable C-J pressure ( $P_{CJ}$ ). The results of two calculations, at  $P_{CJ}$  equal to 40 and 50 kbar, are shown in Fig. 2. The

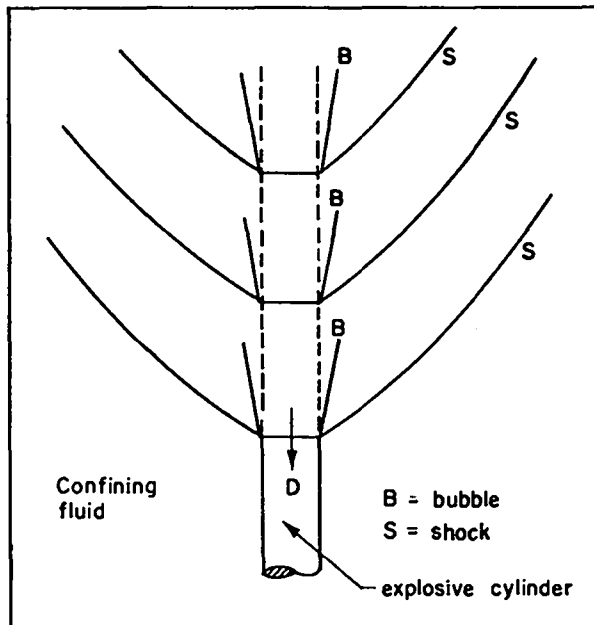


Fig. 1. Successive positions of bubble and shock fronts resulting from a detonation wave of velocity  $D$  propagating down an explosive cylinder immersed in a transparent confining fluid.

differences in bubble-front and shock-front positions in these two calculations are measurable, and we can estimate the accuracy to which  $P_{CJ}$  can be determined from these measurements.

Let  $r$  be the radial position of either the bubble front or the shock front at a fixed position  $z_0$  behind the detonation wave. Let  $z$  be the general coordinate normal to the plane detonation wave front. In general,  $r$  will also be a function of  $P_{CJ}$ , and we can expand  $r(z_0, P_{CJ})$  in a Taylor series for fixed  $z_0$

$$r = r_0 + (\partial r / \partial P_{CJ})_z dP_{CJ} + \dots \quad (1)$$

Thus

$$dP_{CJ} = k \frac{\Delta r}{z_0} \quad (2)$$

where

$$k = z_0 (\partial P_{CJ} / \partial r)_z \quad (3)$$

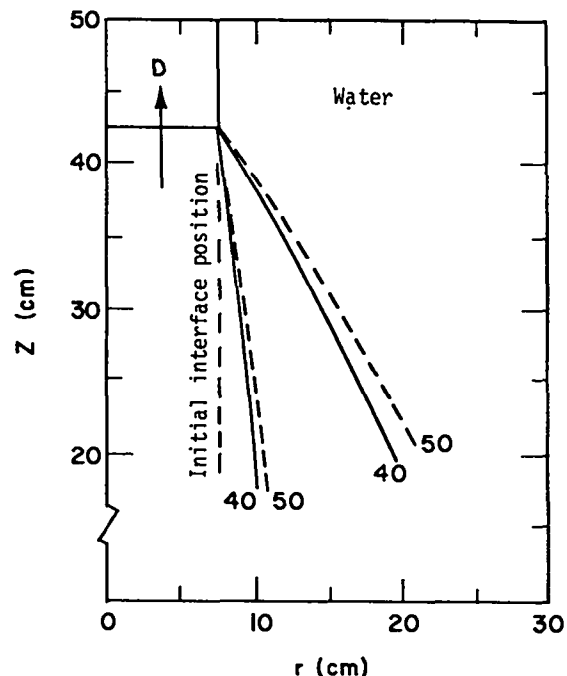


Fig. 2. Comparison of calculated bubble- and shock-front positions using a gamma-law isentrope for the detonation products with  $P_{CJ}$  equal to 40 and 50 kbar. The calculations were made with the 2DL code using a sharp shock burn.

From the calculation results shown in Fig. 2, we find that  $k \cong 150$  kbar for the shock front and  $k \cong 300$  kbar for the bubble front. From Eq. (2), this means that if  $\Delta r$  can be measured to within 0.3 cm at 30 cm behind the detonation front,  $P_{CJ}$  can be determined, in principle, to within 1.5 kbar by measuring the shock front, and to within 3 kbar by measuring the bubble front. Thus, we are better off measuring shock-front positions in determining  $P_{CJ}$  by this method. These results should not be interpreted as giving the absolute accuracy of the technique, but only as indications of the range of errors involved in data interpretation.

An analytical study was also performed to check the previous results concerning sensitivity of bubble-front and shock-front positions to  $P_{CJ}$  at fixed detonation velocity. The results follow. Figure 3 illustrates a plane detonation wave traveling at speed  $D$  parallel to the interface between the explosive and water. Although this analysis only applies specifically to a plane interface between the explosive and water, we assume the results indicate the usefulness of this technique for determining explosive properties in cylindrical geometry.

From elementary principles, the variation of particle velocity  $\underline{u} = (u_1, u_2)$  and the material density  $\rho$  in the centered rarefaction fan behind the detonation front can be written as three coupled ordinary differential equations involving the angle  $\omega$  between a particular centered rarefaction wave and the detonation front. These equations are

$$\frac{du_1}{d\omega} = \left(\frac{c}{\rho}\right) \frac{d\rho}{d\omega} \cos \omega \quad , \quad (4)$$

$$\frac{du_2}{d\omega} = \left(\frac{c}{\rho}\right) \frac{d\rho}{d\omega} \sin \omega \quad , \quad (5)$$

$$\left(\frac{dc}{d\omega} + \frac{c}{\rho}\right) \frac{d\rho}{d\omega} = (u_1 - D) \sin \omega - u_2 \cos \omega \quad , \quad (6)$$

where  $c = (dP/d\rho)^{1/2}$  is the infinitesimal wave velocity at density  $\rho$ , and  $P$  is the pressure ( $P = P_{CJ}$  at  $\omega = 0$ ). Equations (4) through (6) can be solved analytically with a gamma-law isentropic pressure-volume relationship for the detonation products to give the pressure  $P$  and the angle  $\alpha$  through which the interface is bent by the passage of the detonation front. The pressure and angle are then matched with the same calculated quantities in the fluid that result from a shock front propagating at an angle  $\theta$  with respect to the interface. This gives a unique relationship between  $\tan \alpha$ ,  $\tan \theta$ , and  $P_{CJ}$ , or equivalently between  $\tan \alpha$ ,  $\tan \theta$ , and  $\gamma$ , because

$$P_{CJ} = \frac{\rho_0 D^2}{\gamma + 1} \quad , \quad (7)$$

where  $\rho_0$  is the initial density of the explosives. In Fig. 4, the quantities  $\tan \alpha$  and  $\tan \theta$  are plotted as functions of  $\gamma$  for an explosive ( $\rho_0 = 1 \text{ g/cm}^3$  and  $D = 5 \text{ km/s}$ ) in contact with water ( $c_0 = 14.83 \text{ km/s}$  and  $S = 2.0$  in the straight-line  $U_s - u_p$  relationship). From this figure we can estimate the error in  $P_{CJ}$  caused by an error in measuring  $\alpha$  or  $\theta$ . Consider measurement of the interface angle first. The quantity  $\tan \alpha$  can be thought of as a function of  $D$  and  $P_{CJ}$ , or equivalently,  $D$  and  $\gamma$ . Thus

$$d(\tan \alpha) = \left(\frac{\partial \tan \alpha}{\partial \gamma}\right)_D \left(\frac{\partial \gamma}{\partial P_{CJ}}\right)_D dP_{CJ} \quad , \quad (8)$$

when  $D$  is held constant. Thus

$$dP_{CJ} = \frac{\rho_0 D^2}{(1 + \gamma)^2} \left(-\frac{\partial \gamma}{\partial \tan \alpha}\right)_D d(\tan \alpha) \quad . \quad (9)$$

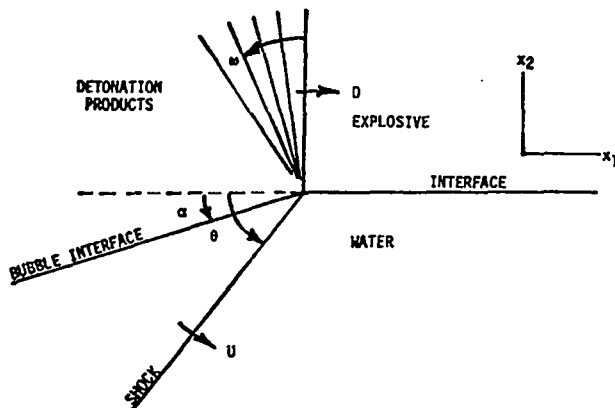


Fig. 3. Detonation wave traveling parallel to the interface between explosive and water. The interface is bent through an angle  $\alpha$  with the passage of the detonation wave.

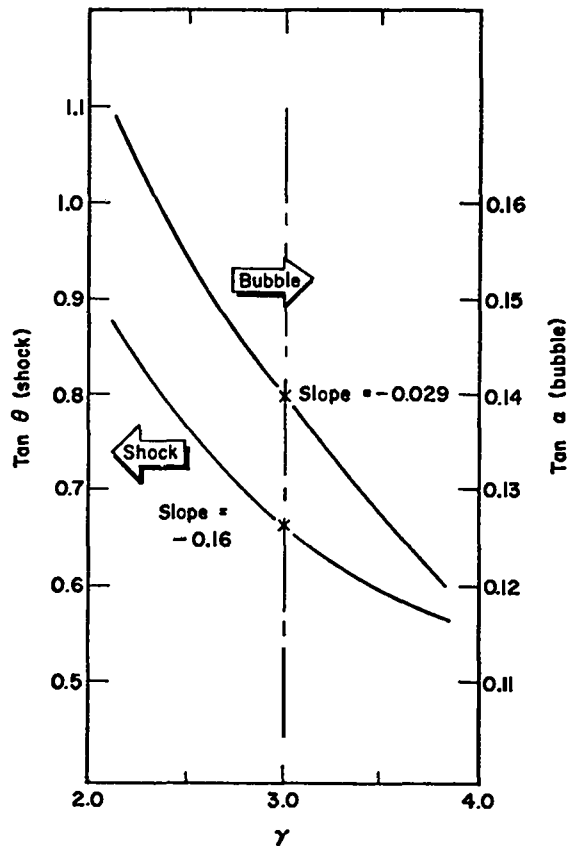


Fig. 4.  $\tan \alpha$  (bubble front) and  $\tan \theta$  (shock front) as functions of  $\gamma$ .

Because  $d(\tan \alpha) = \Delta r/z_0$  in the notation of Eq. (2), Eq. (9) becomes, with use of the slope of the  $\gamma$  vs  $\tan \alpha$  curve in Fig. 4,

$$\Delta P_{CJ} \cong 500 \frac{\Delta r}{z_0} \text{ (kbar)} \quad (10)$$

for the bubble interface. A similar calculation can be performed for the shock-front angle  $\theta$ , with the result that

$$\Delta P_{CJ} \cong 100 \frac{\Delta r}{z_0} \text{ (kbar)} \quad , \quad (11)$$

The conclusion from this sensitivity analysis is that the cylindrical test in water provides useful data for the accurate determination of the C-J pressure in the ideal situation considered here, and that the shock-front position in the water is a better indicator of  $P_{CJ}$  than is the bubble interface

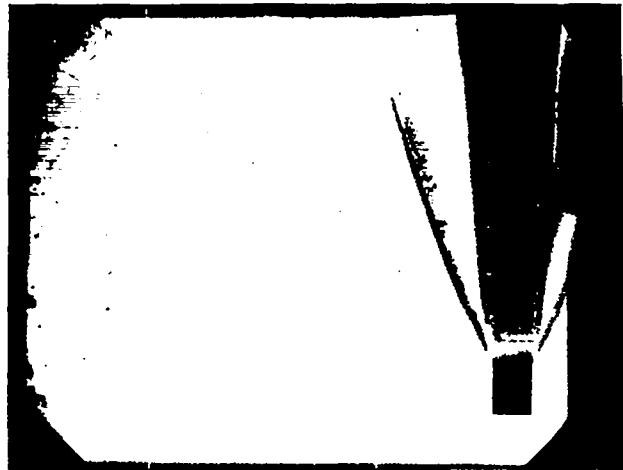


Fig. 5. Shot C-4628; dynamic single exposure of a detonating cylinder of PBX 9407 in water, photographed with a 40-mm I<sup>2</sup>C.

position. We will show later that the interface position is a sensitive indicator of details in the release isentrope of the detonation products.

The second step in determining the usefulness of the proposed experimental measurement is to perform tests with a well-behaved explosive whose properties are known, and compare the results with theoretical predictions based on these known properties. This was done with a 1.27-cm-diam cylinder of PBX 9407 unconfined in water (Fig. 5). The detonation properties of this explosive were calculated with the BKW code,<sup>18</sup> and were then used as input to 2DL to give bubble-front and shock-front positions as functions of time (position  $z_0$  divided by detonation velocity  $D$ ) behind the detonation front.

Details of the BKW calculations and the 2DL code are presented in Refs. 16-18. A comparison of the calculated and measured positions is shown in Fig. 6. The agreement is quite good. Furthermore, the difference between the measured detonation velocity (7.875 km/s) and the BKW-calculated velocity (7.887 km/s) is 0.15%. The agreement between theory and experiment is excellent here, and the results indicate that the water-tank experiments behave as expected.

#### C. Experimental Results for ANFO and WGE-1

Experimental water-tank data of the type described in Secs. III.A and III.B were obtained for  $\sim 10$ -cm (4-in.) and  $\sim 20$ -cm (8-in.) cylindrical

charges of ANFO with both  $\sim 0.6$ -cm (0.25-in.) Plexiglas and  $\sim 1.6$ -cm (0.63-in.) or 2.2-cm (0.87-in.) clay-pipe confinement. Measurements were also made on  $\sim 10$ -cm (4-in.) and  $\sim 20$ -cm (8-in.) cylindrical charges of WGE-1 with  $\sim 1.6$ -cm (0.63-in.) or 2.2-cm (0.87-in.) clay-pipe confinement. The photographic records for these experiments are shown in Figs. 7-11, and representative positions of the shock front in water and interface between confining tube and water are given in Tables IV-VIII.

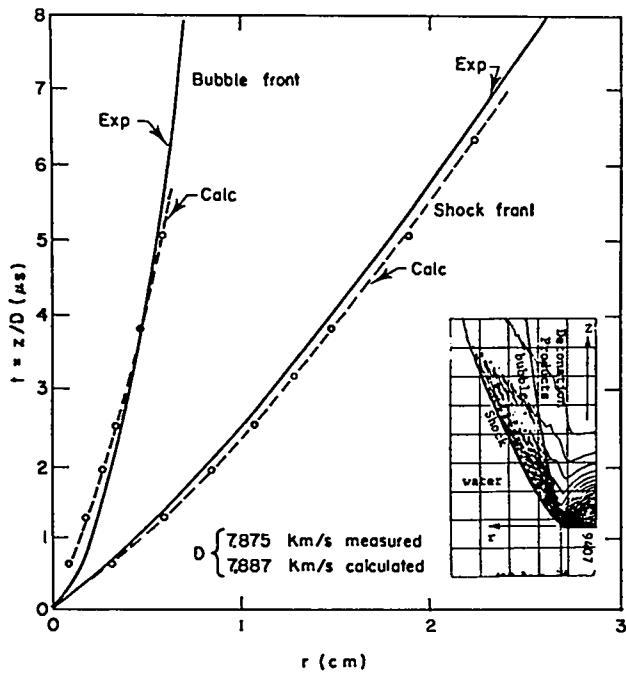


Fig. 6. Experimentally and theoretically determined shock- and bubble-front positions for a 1.27-cm-diam PBX 9407 cylinder in water.

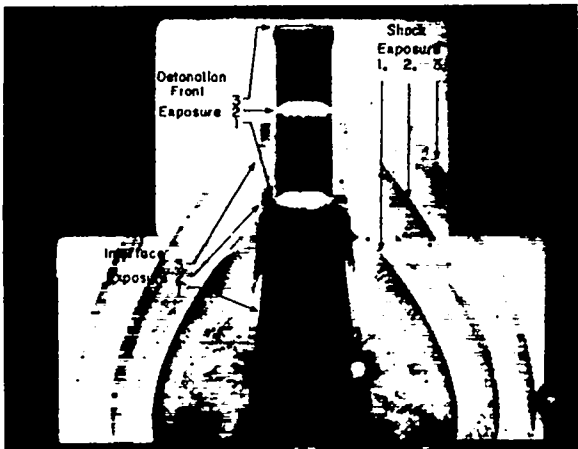


Fig. 7. Shot C-4632; 10-cm-diam ANFO cylinder with Plexiglas confinement.

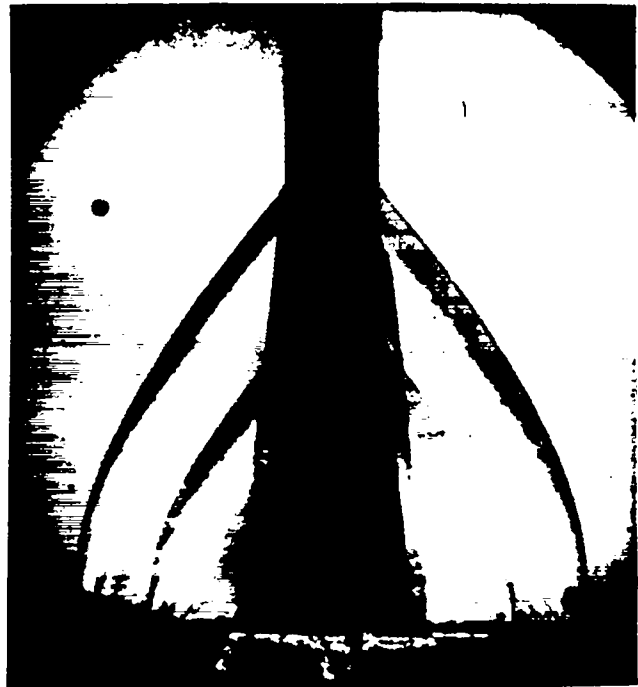


Fig. 8. Shot C-4652; 10-cm-diam ANFO cylinder with clay-pipe confinement.



Fig. 9. Shot C-4664; 20-cm-diam ANFO cylinder with clay-pipe confinement.

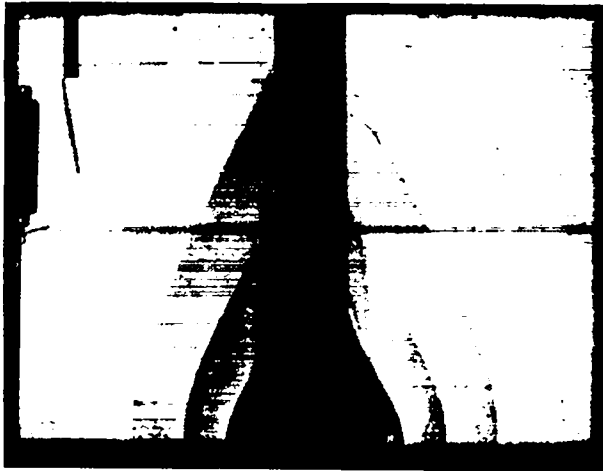


Fig. 10. Shot C-4691; 10-cm-diam WGE-1 with clay-pipe confinement.



Fig. 11. Shot C-4663; 20-cm-diam WGE-1 with clay-pipe confinement.

TABLE IV

EXPERIMENTAL DATA FOR SHOT C-4632<sup>a</sup>

Shock		Interface	
z (cm)	r (cm)	z (cm)	r (cm)
0	5.72	0	5.72
1.26	7.11	11.34	7.96
2.52	8.66	12.60	8.13
5.04	11.14	13.86	8.32
6.31	12.25	15.12	8.46
8.83	14.25	16.39	8.63
12.59	17.07	17.65	8.77
16.39	19.92	18.91	8.89
20.16	22.53	20.16	9.05
25.20	25.33	21.42	9.19
30.25	27.86	23.94	9.48
		25.20	9.64
		30.25	10.18

<sup>a</sup>For ~10-cm-diam ANFO with Plexiglas confinement,  $\rho_0 = 0.95 \text{ g/cm}^3$ ,  $D = 3.48 \text{ km/s}$ .

TABLE V

EXPERIMENTAL DATA FOR SHOT C-4652<sup>a</sup>

Shock		Interface	
z (cm)	r (cm)	z (cm)	r (cm)
0	6.48	0	6.48
0.33	6.72	8.03	7.83
0.56	6.89	11.94	8.20
1.01	7.10	15.87	8.64
1.33	7.31	19.78	9.03
1.77	7.54	23.71	9.43
2.34	7.88	27.63	10.00
2.93	8.37	31.56	10.43
6.87	11.63	35.49	10.73
10.79	14.59	39.42	11.15
14.72	17.48	43.34	11.48
18.64	20.42	47.26	11.94
22.56	22.95	51.18	12.49
26.49	25.37	55.11	13.10
30.41	27.73	59.03	13.43
34.34	29.83		

<sup>a</sup>For ~10-cm-diam ANFO with clay-pipe confinement,  $\rho_0 = 0.90 \text{ g/cm}^3$ ,  $D = 3.47 \text{ km/s}$ .

TABLE VI

EXPERIMENTAL DATA FOR SHOT C-4664<sup>a</sup>

Shock		Interface	
z (cm)	r (cm)	z (cm)	r (cm)
0	12.12	0	12.12
2.03	12.99	15.20	14.73
4.07	14.42	17.24	15.05
6.10	15.99	18.43	15.33
8.14	17.52	19.27	15.36
10.16	19.04	20.46	15.50
12.20	20.55	21.30	15.55
14.23	21.99	22.49	15.83
16.27	23.42	23.34	15.88
18.30	24.79	30.62	16.78
20.33	26.09	34.69	17.25
22.36	27.48	38.76	17.54
24.40	28.81	42.82	17.94
30.49	32.61	48.93	18.61
34.57	35.04	55.03	19.25
40.66	38.57		
44.74	40.76		

<sup>a</sup>For ~20-cm-diam ANFO with clay-pipe confinement,  $\rho_o = 0.90 \text{ g/cm}^3$ ,  $D = 4.12 \text{ km/s}$ .

TABLE VII

EXPERIMENTAL DATA FOR SHOT C-4691<sup>a</sup>

Shock		Interface	
z (cm)	r (cm)	z (cm)	r (cm)
0	6.63	0	6.63
5.11	7.32	2.91	9.54
9.44	7.67	5.82	12.45
13.80	7.96	8.72	15.35
16.71	8.26	11.63	18.26
19.62	8.56	14.52	21.16
22.52	8.91	17.43	24.06
24.28	9.27	20.34	26.97
		23.25	29.88
		24.08	30.71

<sup>a</sup>For ~10-cm-diam WGE-1 with clay-pipe confinement,  $\rho_o = 1.47 \text{ g/cm}^3$ ,  $D = 4.53 \text{ km/s}$ .

TABLE VIII

EXPERIMENTAL DATA FOR SHOT C-4663<sup>a</sup>

Shock		Interface	
z (cm)	r (cm)	z (cm)	r (cm)
0	12.14	0	12.14
8.0	13.1 <sup>b</sup>	2.44	13.13
16.0	14.1 <sup>b</sup>	4.89	14.42
24.0	15.0 <sup>b</sup>	7.32	15.69
32.0	15.9 <sup>b</sup>	9.76	17.14
37.97	16.72	12.20	18.55
40.42	17.03	14.64	19.74
42.85	17.22	17.08	20.97
45.28	17.54	19.52	22.30
47.73	17.86	21.96	23.54
50.18	18.03	24.40	24.88
52.60	18.17	26.84	26.04
55.05	18.37	29.28	27.37
57.49	18.73	31.72	28.63
59.93	18.94	34.15	29.81
69.68	19.74	36.60	31.08
		39.04	32.30
		41.48	33.54
		43.91	34.73
		46.35	35.92
		48.80	37.01
		51.24	54.02

<sup>a</sup>For ~20-cm-diam WGE-1 with clay-pipe confinement,  $\rho_o = 1.50 \text{ g/cm}^3$ ,  $D = 4.81 \text{ km/s}$ .

<sup>b</sup>Linear interpolation.

For shots C-4632 (10-cm-diam ANFO with Plexiglas confinement) and C-4652 (10-cm-diam ANFO with clay-pipe confinement), the detonation velocities are almost identical: 3.48 km/s and 3.47 km/s, respectively. This indicates that details of the type of confinement are not important in this configuration, as long as the sound speed in the confining medium is less than the detonation velocity. In fact, we conclude that the confinement provided by both the Plexiglas/water and clay/water systems is equivalent to an infinite medium with mechanical properties representative of typical rocks. It may

be argued that the agreement in detonation velocity between shots C-4632 (Plexiglas confinement) and C-4652 (clay-pipe confinement) is a consequence of the density difference of 5%. In principle the density difference may be a factor, but it is not considered to be significant in actual field applications where density variations of this magnitude are commonplace. Also note that the measured detonation velocity is somewhat less than the value of 3.9 km/s measured by Helm et al.<sup>7</sup> for a 10-cm-diam charge.

Based on ideal performance calculations using the BKW code,<sup>18</sup> the detonation velocity for ANFO should be 5.44 km/s with a detonation pressure of 73.4 kbar, if the reaction were complete. Comparison with the measured detonation speed shows that conditions are far from ideal. When we go to 20 cm in experiment C-4664, the detonation velocity increases to 4.12 km/s. Conditions are tending toward ideal, but still have a substantial way to go. Measurements made by Helm et al.<sup>7</sup> show that detonation velocities in ANFO are also well below ideal conditions for charge diameters of 5.1 cm, 10.2 cm, and 29.2 cm. In fact, field data<sup>7</sup> on a 550-cm charge of ANFO give a detonation velocity of only 4.7 km/s. Hence, even for extremely large charges, the detonation velocity remains considerably below the value predicted by the BKW code under the assumption of complete reaction. Persson,<sup>14</sup> however, reports detonation velocities in ANFO very close to the theoretical value of 5.44 km/s for 26.8-cm charges confined in rock.

Therefore, we concluded that the detonation velocity data obtained on 10- and 20-cm-diam ANFO charges are consistent with existing data, and that reactions in these geometries are nonideal.

Experimental data for 10- and 20-cm charges of WGE-1 are given in Tables VII and VIII. Based on complete reaction of this explosive, the predicted detonation velocity is 7.34 km/s with a detonation pressure of 187.2 kbar. Comparison with the experimentally determined detonation velocities of 4.53 km/s and 4.81 km/s shows that this explosive system is also nonideal.

A discussion of nonideal explosives, their theoretical description, and comparison of water-tank data with two-dimensional Lagrangian hydrodynamic calculations based on theoretical equations

of state for ANFO and WGE-1 are presented in the next section.

#### IV. NONIDEAL EXPLOSIVES AND THEORETICAL SIMULATION OF THE WATER-TANK EXPERIMENTS

Mader<sup>11</sup> defines a nonideal explosive as one having a C-J pressure, velocity, or expansion isentrope significantly different than expected from equilibrium, steady-state calculations such as BKW.<sup>18</sup>

For example, an experimentally determined detonation velocity of 7.55 km/s is observed for AmateX/40 ( $\rho_0 = 1.66 \text{ g/cm}^3$ ), whereas a BKW calculation gives a value of 7.96 km/s based on complete reaction of the AN. Mader showed that if the AN was assumed to be a compressible inert solid, the BKW calculation gave a detonation velocity of 7.15 km/s, somewhat below the experimentally observed value. Therefore, it was concluded that some degree of AN reaction was occurring. In fact, it was found that if 50% of the AN underwent reaction, the calculated detonation velocity was 7.57 km/s, within 0.3% of the measured value. Hugoniot for 0, 50, and 100% AN reaction are shown in Fig. 12 along with the experimentally determined Rayleigh line for AmateX/40.

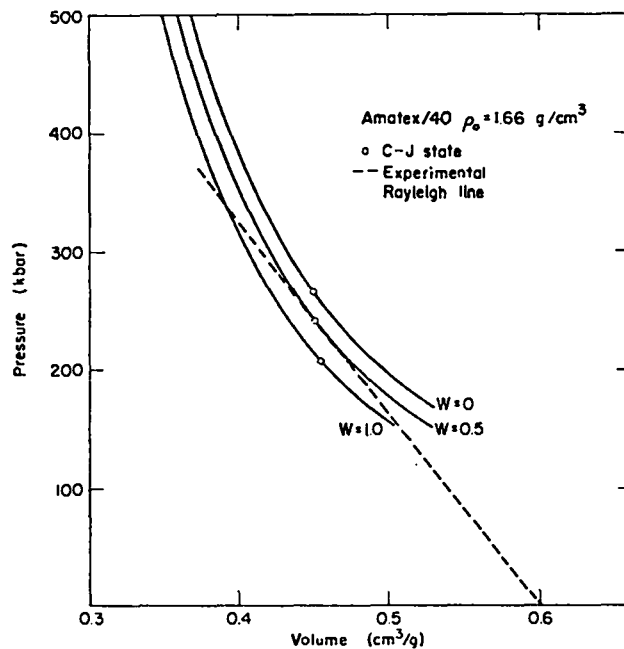


Fig. 12. The BKW-calculated Hugoniot for AmateX/40 ( $W$  is the mass fraction of AN that remains unreacted).

We apply the same ideas to the performance of ANFO and WGE-1 to determine the degree of reaction at the C-J plane. In addition, comparison of calculated shock and pipe/water interface positions with water-tank data gives information on when and where additional reaction takes place.

#### A. ANFO

For 10-cm-diam charges of ANFO confined with either 0.6-cm Plexiglas or 1.6-cm clay pipe (shots C-4632 and C-4652), the measured detonation velocity was approximately 3.5 km/s. This is well below the theoretical BKW-determined detonation velocity of 5.4 km/s for complete reaction. The C-J pressure corresponding to complete detonation of ANFO is 73 kbar. These data indicate that some portion of the candidate reactants remains inert at the C-J plane. If we assume that 55% of the AN remains inert, a BKW calculation gives a detonation velocity of 3.5 km/s, in agreement with experimental data. The corresponding C-J pressure is 24 kbar. Not only do we obtain the C-J pressure and the detonation velocity from the BKW calculation, but also the release isentrope passing through the C-J point. From this information an equation of state of the detonation products is constructed and used in a 2DL calculation<sup>16,17</sup> to simulate the water-tank shots C-4632 and C-4652. When we compare the computed response of shot C-4632 with the data, we find that both the measured shock-wave and Plexiglas/water interface positions are in poor agreement with the calculation, as shown in Fig. 13.

We then sought an explanation for this discrepancy. An obvious consideration in this type of experiment is the optical refraction effect resulting from the shock compression of the water surrounding the encased cylindrical charge. The curved shock front acts as a lens that makes the radial position of the expanding cylinder appear greater than it actually is. This effect is analyzed in detail in the Appendix; it is found to be too small to account for the difference between theory and experiment shown in Fig. 13.

Another possible explanation for the discrepancy is that the remaining inert AN at the C-J plane undergoes reaction behind the detonation front. Several BKW calculations were performed to determine the release isentrope from the 24-kbar C-J point under the assumption that the AN continues to react.

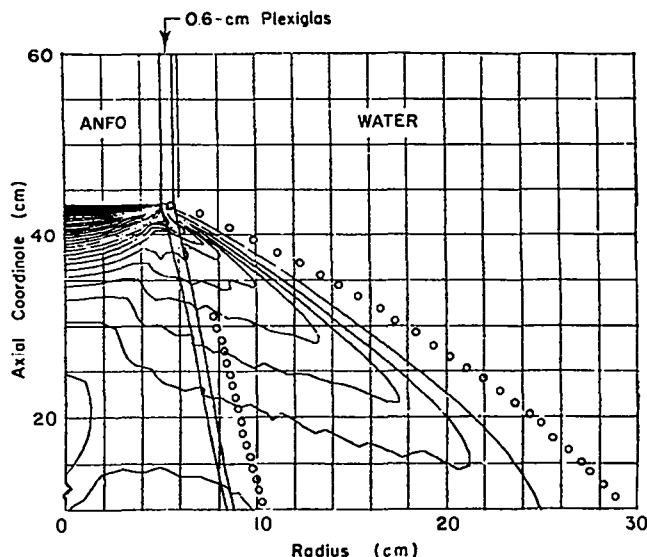


Fig. 13. Shot C-4632; comparison of measured (circles) shock and interface positions with those calculated assuming that 55% of the AN remains inert behind the detonation front. The contours are the calculated pressures at 1-kbar intervals.

Based on the assumption that all of the remaining (55%) AN is reacted by the time the pressure has dropped to 10 kbar behind the detonation wave, a new release isentrope is calculated and used in a second calculation of water-tank shot C-4632. Figure 14 shows the results. Note that both the shock and interface positions agree better with the experimental data. These results are not sensitive to the precise way in which the remaining AN is assumed to undergo reaction. Numerous two-dimensional calculations were performed with various additional AN reactions and all results were identical to those shown in Fig. 14.

A computer simulation of shot C-4652 was run to see if the results we have just presented depend on the details of confinement. In shot C-4652, 10 cm of ANFO was confined with 1.6 cm of clay pipe ( $\rho_0 = 2.3 \text{ g/cm}^3$  and bulk modulus is 168 kbar) in place of Plexiglas. Figure 15 shows the results of calculations based on the same explosive equation of state used in the calculations of Fig. 14. Because of the good agreement, we again concluded that Plexiglas and clay-pipe confinement are approximately equivalent and that ANFO performance is not very sensitive to the confinement details in the 10-cm configuration.

In addition, an "end-on air-shock experiment" was conducted to provide an independent check of

these results. In this experiment, a relatively short, 10-cm-diam ANFO cylinder was detonated from one end, and the velocity of the resulting air shock was measured as the nearly plane detonation wave reached the opposite end of the cylinder. The experimental record is shown in Fig. 16 as three

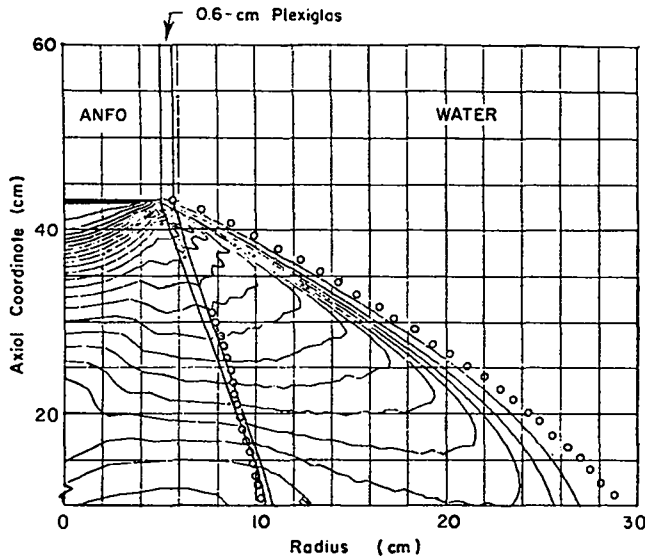


Fig. 14. Shot 4632; comparison of measured (circles) shock and interface positions with those calculated assuming that all of the remaining (55%) AN reacts by the time the pressure drops to 10 kbar. The contours are the calculated pressures at 1-kbar intervals.

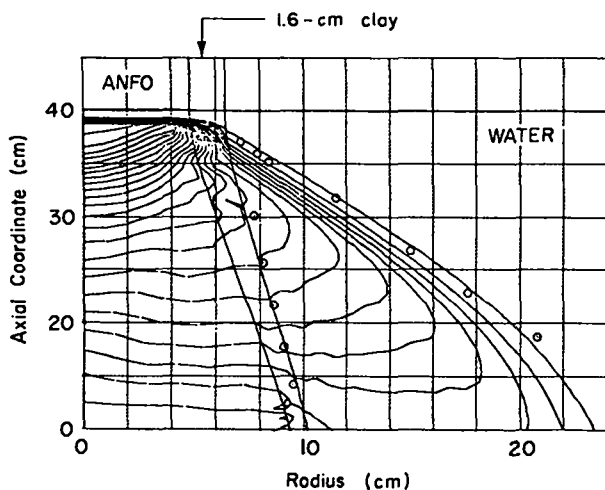


Fig. 15. Shot C-4652; comparison of measured (circles) shock and interface positions with those calculated with the same explosive equation of state used in Fig. 14. The contours are the calculated pressures at 1-kbar intervals.

exposures of the shock wave in air after the detonation has reached the end of the cylinder.

If we know the air Hugoniot, we can establish a single pressure/particle-velocity state for the detonation products. This state is shown in Fig. 17 with the three release isentropes for ANFO corresponding to complete reaction, 55% inert AN with no additional burn to completion, and 55% inert AN with

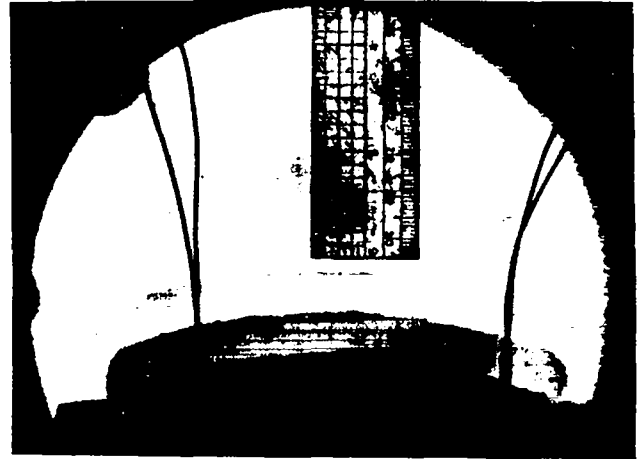


Fig. 16. Shot C-4655; three exposures of air shock induced from the end of a 10-cm-diam ANFO cylinder.

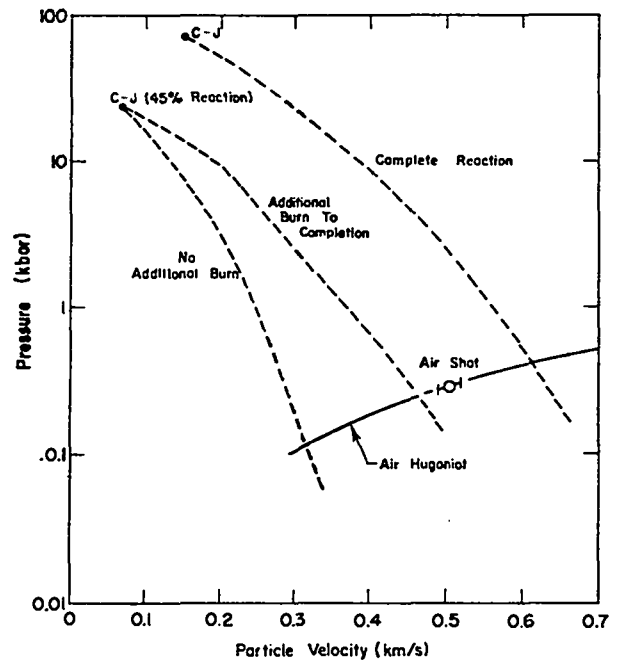


Fig. 17. Release isentropes for ANFO for complete reaction, 45% AN reaction, and 45% AN reaction with additional burn. Also shown is the experimentally determined point on the air Hugoniot from shot C-4655.

additional burn to completion. It is clear from Fig. 17 that the air-shot data are in good agreement with the assumption of 45% AN reaction at the C-J plane followed by additional burn to completion.

Table VI gives results for a 20-cm-diam ANFO charge in clay pipe surrounded by water. The measured detonation velocity of 4.1 km/s is greater than the 3.5-km/s velocity for the 10-cm-diam charge but still considerably less than the theoretical value of 5.4 km/s based on complete reaction. If we assume that 38% of the AN remains inert at the C-J plane, a BKW calculation predicts a detonation velocity of 4.1 km/s and a C-J pressure of 36 kbar. Figure 18 shows the results of a 2DL calculation of shot C-4664 assuming the remaining 38% AN undergoes reaction close behind the C-J plane. The calculated position of the shock front agrees well with the data, but the clay/water interface does not. The calculated interface position is parallel to the measured position but at a smaller radius. This may indicate a physical shortcoming in the way the additional energy release is calculated. Here we have been treating it as a rate-independent process by varying the release isentrope. Perhaps a more sophisticated method of rate-dependent energy release would give the confining pipe a greater initial

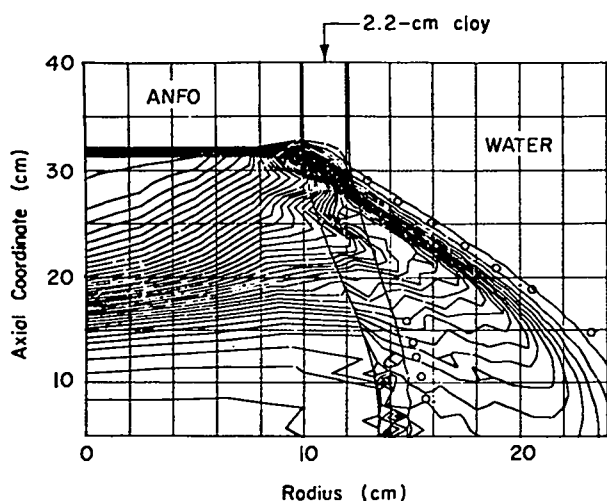


Fig. 18. Shot C-4664; comparison of measured (circles) shock and interface positions with those calculated assuming that 38% AN is inert at the C-J plane but reacts within a few tens of microseconds later. The contours are the calculated pressures at 1-kbar intervals.

acceleration in better agreement with experimental observation. This remains to be investigated.

#### B. WGE-1

Water-tank shots C-4663 (20-cm-diam) and C-4691 (10-cm-diam) conducted on WGE-1 were described in Sec. III.C. For the 20-cm-diam charge, the detonation speed was 4.81 km/s, well below the ideal detonation speed of 7.3 km/s at a C-J pressure of 187 kbar. Therefore, we conclude that this explosive's performance is nonideal and can be treated in the same way as that for ANFO. A BKW calculation for this explosive gives a C-J pressure of 71 kbar and a detonation velocity of 4.95 km/s under the assumption that none of the AN reacts (this explosive is 46 wt% AN). This velocity is slightly greater than that measured experimentally, which implies that perhaps even some of the other constituents do not undergo complete reaction. Because the calculated value of 4.95 km/s is reasonably close to the measured detonation velocity, we did not try to refine the calculation.

We chose to limit the reaction of the AN rather than that of some of the other constituents because AN reaction actually reduces the C-J temperature as a result of the way energy is partitioned between potential and kinetic contributions. A heuristic way of picturing this is to consider both the positive heat of reaction of AN and the change in heat capacity of the reaction products caused by additional AN reaction. If the heat capacity increased fast enough, it could offset the effect of the heat of reaction that is causing the temperature to increase. This is what happens for AN.

If we assume that none of the AN reacts at the C-J plane and that the AN remains inert behind the detonation wave, a 2DL calculation is compared with the experimental data for shot C-4663. The results presented in Fig. 19 show very good agreement between theory and experiment for both shock and interface positions. Thus, we conclude that, on the time scale of this shot at least, the AN in WGE-1 does not react at all.

To examine the effect of additional reaction on the computed shock and interface positions, a second calculation was run in which it was assumed that all of the AN reacted within a few microseconds

behind the C-J plane. The results of this calculation in comparison with measured values are shown in Fig. 20. Additional AN reaction has a significant effect on the measured positions; therefore we conclude that if this reaction had occurred, it would have been observed experimentally.

## V. CONCLUSIONS

The results of the experimental measurements and theoretical analyses presented here have shown that the water-tank technique is very useful in determining the nonideal explosive properties of commercial explosives. The specific conclusions that have been reached concerning ANFO and WGE-1 follow.

- A 10-cm-diam cylinder of ANFO with either Plexiglas or clay-pipe confinement has a detonation velocity of  $\sim 3.5$  km/s, corresponding to 55% AN remaining inert at the C-J plane. The calculated C-J pressure is 24 kbar (compared to 71 kbar for an ideal reaction). The remaining 55% AN undergoes reaction within a few microseconds behind the C-J plane.
- A 20-cm-diam cylinder of ANFO with clay-pipe confinement has a detonation velocity of  $\sim 4.1$  km/s, corresponding to 38% AN remaining inert at the C-J plane. The calculated C-J pressure is 36 kbar.

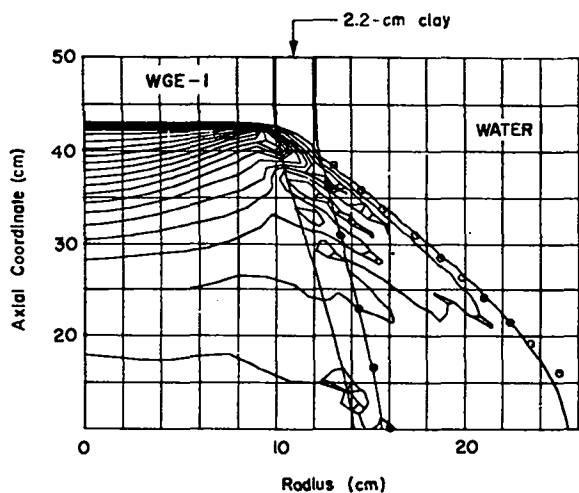


Fig. 19. Shot C-4663; comparison of measured (circles) shock and interface positions with those calculated assuming that none of the AN reacts during the experiment ( $\sim 60 \mu\text{s}$ ). The contours are calculated pressures at 5-kbar intervals.

The remaining 38% AN undergoes reaction within a few microseconds behind the detonation front. Detailed agreement between theory and data is not as good for shot C-4664 as for the others, possibly because of the elementary rate-independent way in which additional reaction was treated theoretically; that is, by simply modifying the release isentrope to reflect the higher pressures maintained to greater specific volumes. More sophisticated treatments of rate-dependent energy release may rectify this problem.

- A 20-cm-diam cylinder of WGE-1 had a detonation velocity of  $\sim 4.8$  km/s, corresponding to all of the AN remaining inert at the C-J plane. The calculated C-J pressure is 71 kbar (compared to 187 kbar for an ideal reaction). The experimental evidence is that the AN constituent does not undergo reaction during the experiment ( $>60 \mu\text{s}$ ).
- A 10-cm-diam cylinder of WGE-1 had a detonation velocity of  $\sim 4.5$  km/s, indicating that even less reaction occurred. Because 10 cm is near the unconfined failure diameter for this explosive, no attempt was made to simulate the experiment numerically for estimating which constituents were inhibited from reaction.

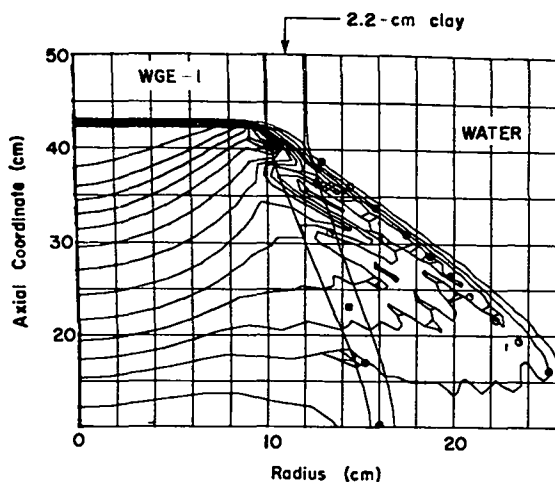


Fig. 20. Shot C-4663; comparison of measured (circles) shock and interface positions with those calculated assuming that none of the AN reacts at the C-J plane but does within a few microseconds behind the detonation wave. The contours are calculated pressures at 5-kbar intervals.

ACKNOWLEDGMENTS

The authors acknowledge the assistance and suggestions of W. J. Carter in the planning of these

experiments and W. C. Davis in the analysis of the index-of-refraction effects.

APPENDIX

INDEX-OF-REFRACTION EFFECTS

Lack of agreement between the calculated and experimentally determined Plexiglas/water interface prompted the following three-dimensional analysis of refraction effects in the water-tank experiments. This analysis begins with the following definition of terms in reference to Fig. A-1.

- r = bubble radius (at distance  $z_0$  behind detonation)
- R = shock radius (at distance  $z_0$  behind detonation)
- $\hat{n}$  = unit vector normal to shock front at E
- $\alpha$  = angle between the shock front and cylinder axis
- $\hat{i}$  = unit vector parallel to x-axis: the camera is located at infinity along the positive x-axis
- $\theta$  = angle between  $\hat{n}$  and  $\hat{i}$  (the angle of refraction)
- $\theta'$  = the angle of incidence
- $\hat{m}$  = unit vector normal to the plane defined by  $\hat{n}$  and  $\hat{i}$ :  $\hat{m} = \hat{n} \times \hat{i}$
- $\delta r$  = error in locating r of bubble interface
- $\delta z$  = error in locating z of bubble interface
- D = scalar distance between the apparent and true positions of a point on the bubble front
- $\phi$  = angle between  $\hat{m}$  and z-axis

The first step in calculating  $\delta r$  and  $\delta z$  is defining the unit vector  $\hat{n}$ , normal to the shock front at point E in Fig. A-1. This can be done by noting that the equation for the cone tangent to the shock front at a distance  $z_0$  behind the detonation front is

$$f(x,y,z) = \sqrt{x^2 + y^2} - z \tan \alpha = \text{constant}, \quad (A-1)$$

and the normal  $\hat{n}$  is in the direction  $\nabla f$ . Thus

$$\nabla f = (x/R, y/R, -\tan \alpha) \quad (A-2)$$

We evaluate this vector function at  $x = \overline{AE} = R\sqrt{1 - (r/R)^2}$  and  $y = -r$ , with the result that

$$\hat{n} = \cos \alpha (\sqrt{1 - (r/R)^2}, -r/R, -\tan \alpha) \quad (A-3)$$

Because  $\hat{i} = (1,0,0)$ , the unit vector  $\hat{m} = \hat{n} \times \hat{i}$  and the angle  $\theta$  are easily found to be

$$\hat{m} = \cos \alpha (0, -\tan \alpha, r/R) \quad (A-4)$$

$$\cos \theta = \cos \alpha \sqrt{1 - (r/R)^2} \quad (A-5)$$

Because  $\theta'$  and  $\theta$  are the angles of incidence and refraction, we find

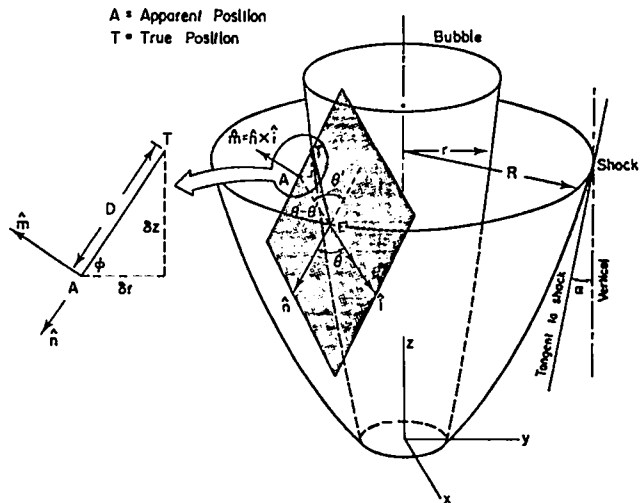


Fig. A-1. Location of apparent and true positions of bubble interface as viewed by observer located at a great distance (compared to R) along the positive x-axis.

$$\theta' = \sin^{-1} \left( \frac{n_0}{n} \sin \theta \right) , \quad (A-6)$$

which can be expanded in a Taylor series in  $n$  about  $n_0$  (because the difference between  $n$  and  $n_0$  is very small),

$$\theta' \cong \theta - \frac{\sin \theta}{\sqrt{1 + \sin^2 \theta}} (n - n_0) . \quad (A-7)$$

Therefore, to a very good approximation, the difference between  $\theta$  and  $\theta'$  is given by

$$\theta - \theta' \cong \frac{\sin \theta}{\sqrt{1 + \sin^2 \theta}} (n - n_0) . \quad (A-8)$$

Because this angular variation is small, the line segment  $\overline{AT} = D$  in Fig. A-1 is given by

$$\overline{AT} = D \cong \overline{AE} (\theta - \theta') , \quad (A-9)$$

or

$$D \cong \frac{R \sqrt{1 - (r/R)^2} \sin \theta}{\sqrt{1 + \sin^2 \theta}} (n - n_0) . \quad (A-10)$$

From Eqs. (A-4) and (A-10) it is now very easy to determine  $\delta r$  and  $\delta z$ . Because

$$\cos \phi = \hat{m} \cdot (0, 0, 1) , \quad (A-11)$$

we find that

$$R \cos \phi = r \cos \alpha , \quad (A-12)$$

and therefore

$$\delta r = D \cos \phi = \frac{r \sqrt{1 - (r/R)^2}}{\sqrt{1 + \sin^2 \theta}} \cos \alpha \sin \phi (n - n_0) , \quad (A-13)$$

$$\delta z = D \sin \phi = \frac{R \sqrt{1 - (r/R)^2}}{\sqrt{1 + \sin^2 \theta}} \sin \phi \sin \theta (n - n_0) , \quad (A-14)$$

or

$$\frac{\delta r}{r} = N \cos \alpha , \quad (A-15)$$

$$\frac{\delta z}{R} = N \sin \phi , \quad (A-16)$$

$$N = \frac{\sqrt{1 - (r/R)^2}}{\sqrt{1 + \sin^2 \theta}} \sin \theta (n - n_0) . \quad (A-17)$$

From the initial calculation of the ANFO/Plexiglas/water experiment we find that at  $z = 25$  cm behind the detonation front (see Fig. A-2),  $r = 8$  cm,  $R = 25$  cm,  $\alpha = 30^\circ$ , and the average volume is  $\sim 0.92$  cm<sup>3</sup>/g. The index of refraction of water<sup>19</sup> is  $n_0 = 1.34$  at a specific volume of 1 cm<sup>3</sup>/g. Dorsey<sup>19</sup> refers to the work of Quincke<sup>20</sup> in which he found that the product of  $(n - 1)$  and the specific volume  $v$  was nearly constant. Thus

$$(n - 1)v \cong (n_0 - 1)v_0 \quad (A-18)$$

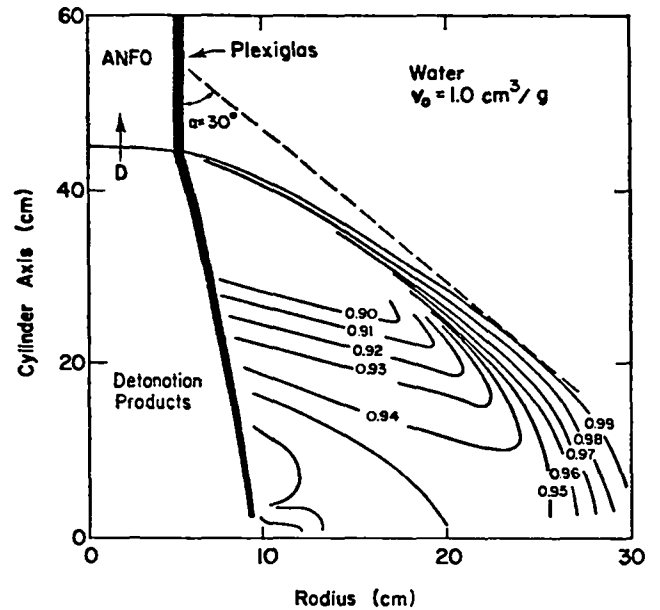


Fig. A-2. Calculation of the ANFO/Plexiglas/water experiment. Contour lines are specific volume  $v$  in cm<sup>3</sup>/g. At a distance of  $\sim 25$  cm behind the detonation front, the shock wave makes an angle of  $\sim 30^\circ$  to the cylinder axis.

or

$$(n - n_0) \cong (n_0 - 1) \left( \frac{v_0}{v} - 1 \right) \cong 0.03 \quad . \quad (A-19)$$

From these values we find that  $\delta r/r \cong 0.012$  and  $\delta z \cong 0.34$  cm; that is, the corrections in this case are fairly small. Certainly they are not large enough to account for the differences between theory and experiment shown in Fig. 13.

For completeness, we have applied the analysis presented here to the data given in Table III. From Fig. A-2, we can estimate the average specific volume behind the shock front as a function of  $z$  (the distance behind the detonation front in the ANFO). Then, with the use of Eq. (A-18), the average index-of-refraction change can be found. The result is expressed mathematically as

$$n - n_0 \cong 0.093 e^{-(z/15)} + 0.020 \quad , \quad (A-20)$$

where  $n_0 = 1.34$  and  $z$  is in centimeters. With this variation of index of refraction, the data on bubble-front position given in Table IV are corrected as shown in Table A-I. This correction is clearly much smaller than the difference between theory and experiment in Fig. 13.

#### REFERENCES

1. C. H. Noren and D. D. Porter, "A Comparison of Theoretical Explosive Energy and Energy Measured Under Water with Measured Rock Fragmentation," in Advances in Rock Mechanics, Vol. III, Part B, (Nat. Acad. Sci., 1974).
2. W. I. Duvall and T. C. Atchison, "Rock Breakage by Explosives," US Bureau of Mines report R.I. 5336 (1957).
3. U. Langefors and V. Kihlstrom, The Modern Technique of Rock Blasting (John Wiley and Sons, Inc., New York, 1963).
4. C. H. Johansson and P. A. Persson, Detonics of High Explosives (Academic Press, New York, 1970).
5. P. A. Persson, N. Lundberg, and C. H. Johansson, "The Basic Mechanisms in Rock Blasting," in Proc. 2nd Cong. Int. Soc. Rock Mech. (Beograd, 1970), p. 1.
6. E. L. Lee, H. C. Hornig, and J. W. Kury, "Adiabatic Expansion of High Explosive Detonation Products," Lawrence Livermore Laboratory report UCRL-50422 (May 1968).

TABLE A-I

CORRECTED  $z$  AND  $r$  POSITIONS OF THE PLEXIGLAS/WATER INTERFACE FROM REFRACTION EFFECTS CAUSED BY LIGHT PASSING THROUGH THE SHOCK WAVE IN WATER

Original Data		Corrected Data	
$z$ (cm)	$r$ (cm)	$z$ (cm)	$r$ (cm)
0.0	5.72	0.0	5.72
11.34	7.96	11.82	7.76
12.60	8.13	13.08	7.93
13.86	8.32	14.36	8.14
15.12	8.46	15.60	8.27
16.39	8.63	16.87	8.45
17.65	8.77	18.13	8.59
18.91	8.89	19.38	8.73
20.16	9.05	20.61	8.89
21.42	9.19	21.87	9.03
22.68	9.32	23.12	9.17
23.94	9.48	24.35	9.34
25.20	9.64	25.61	9.49
26.47	9.76	26.88	9.61
27.72	9.93	28.11	9.79
28.99	10.04	29.37	9.91
30.25	10.18	30.63	10.05

7. F. Helm, M. Finger, B. Hayes, E. Lee, H. Cheung, and T. Walton, "High Explosive Characterization for the Dice Throw Event," Lawrence Livermore Laboratory report UCRL-52042 (June 1976).
8. L. Penn, F. Helm, M. Finger, and E. Lee, "Determination of Equation-of-State Parameters for Four Types of Explosive," Lawrence Livermore Laboratory report UCRL-51892 (August 1975).
9. J. Hershkowitz and J. Rigdon, "Evaluation by a Modified Cylinder Test of Metal Acceleration by Nonideal Explosives Containing Ammonium Nitrate," Picatinny Arsenal report PA-TR-4611 (April 1974).
10. N. L. Coleburn, H. D. Jones, and H. M. Sternberg, "Initiation, Detonation Propagation, Computational Studies for Submunitions Containing Amatex-20," Naval Surface Weapons Center report TR 75-94, White Oak Laboratory (February 1976).
11. C. L. Mader, "An Equation of State for Nonideal Explosives," Los Alamos Scientific Laboratory report LA-5864 (April 1975).
12. M. Finger, F. Helm, E. Lee, R. Boat, H. Cheng, J. Walton, B. Hayes, and L. Penn, "Characterization of Commercial Composite Explosives," Proc. Symp. Detonation, 6th, August 1976, pp. 188-196.
13. M. W. McKay, S. L. Hancock, and D. Randall, "Development of a Low-Density Ammonium Nitrate/Fuel Oil Explosive and Modeling Its Detonation Properties," Defense Nuclear Agency report DNA-3351F (October 1974).

14. P. A. Persson, "Swedish Methods for Mechanized Blasthole Charging," AIME Preprint No. 75-AO-74 (1975).
15. O. G. Winslow, W. C. Davis, and W. C. Chiles, "Multiple-Exposure Image-Intensifier Camera," Proc. Symp. Detonation, 6th, August 1976, pp. 197-200.
16. C. L. Mader, Numerical Modeling of Detonations (University of California Press, Berkeley, CA, 1978).
17. C. L. Mader, "The Two-Dimensional Hydrodynamic Hot Spot - Volume III," Los Alamos Scientific Laboratory report LA-3450 (April 1966).
18. C. L. Mader, "FORTRAN BKW: A Code for Computing the Properties of Explosives," Los Alamos Scientific Laboratory report LA-3704 (July 1967).
19. N. E. Dorsey, Properties of Ordinary Water Substance (Reinhold Publishing Corp, New York, 1940), p. 281.
20. G. Quincke, "Ueber die Beziehungen Zwischen Compressibilität und Brechungsexponenten von Flüssigkeiten," Ann. d. Physik (Wied.) 44, 774-777 (1891).